identical to that shown in Fig. 4.

Regarding diffusional atomic jumps at high temperature, it is natural to consider that the local vibration anomalies enhance the short-range diffusion of atoms located around the cluster centre with a help of a phason-site-mediated transport mechanism, causing occasional diffusion jumps of not only Al but also TM atoms into the phason β site. This explains a random occurrence of five-fold symmetry-like clusters at some places (Fig. 1b). Note that the atoms delivered to the β site by diffusion jump can be quenched in, so that they will be recognized as 'quenched phason-defects' (including chemical and site-occupation disorders that are significant at the core of the 2-nm clusters), which have in fact been detected by experimental measurements on the quenched sample[20,27,28].

Alternatively, five-fold-symmetric 2-nm clusters emerge as the thermodynamically stable configuration when the present high-temperature $Al_{72}Ni_{20}Co_8$ undergoes phase transition at lower temperatures ($\lesssim 990$ K, to a less-quasiperiodic ordered phase); this suggests that the phason β sites, metastable at high temperature, provide stable positions for TM atoms at low temperature. This also indicates that the above structural transition is closely related to phason-related atomic behaviour, which is significant at the centre of the 2-nm clusters, as shown in the present direct observation. □

Methods

Atomic-resolution images were taken by 200-kV (JEOL 2010F) and 300-kV (VG Microscopes, HB603U) scanning transmission electron microscopes, providing a minimum probe of approximately 0.150 nm and 0.126 nm, respectively. The former microscope was used for a high-temperature *in situ* observation. Specimens were prepared by crushing the bulk material and depositing it onto perforated amorphous carbon film supported on Cu grids; by this method, the surface amorphous layer, roughness, and contamination that are frequently induced by ion-milling and which strongly affect image contrast, can be avoided. Thus, the intensities measured from the present images give reliable information. Heating to 1,100 K in the microscope was achieved within 5 min, which effectively suppresses a phase transition that would occur at $\lesssim 990$ K during heating. The electron diffraction pattern taken at 1,100 K from the grain used for imaging (Fig. 1) confirmed that $Al_{72}Ni_{20}Co_8$ retains its basic AlNiCo structure during *in situ* high-temperature observation. Energy-dispersive X-ray spectroscopy showed no detectable compositional change of the grain before and after the heat treatment in the microscope.

Received 20 September; accepted 25 November 2002; doi:10.1038/nature01337.

1. Bak, P. Phenomenological theory of icosahedral incommensurate ("quasiperiodic") order in Mn-Al alloys. *Phys. Rev. Lett.* **54,** 1517–1519 (1985).
2. Janssen, T. Crystallography of quasi-crystals. *Acta Crystallogr. A* **42,** 261–271 (1986).
3. Yamamoto, A. Crystallography of quasiperiodic crystals. *Acta Crystallogr. A* **52,** 509–560 (1996).
4. Socolar, T., Lubensky, T. & Steinhardt, P. J. Phonons, phasons, and dislocations in quasicrystals. *Phys. Rev. B* **34,** 3345–3360 (1986).
5. Jaric, M. V. & Nelson, D. R. Diffuse scattering from quasicrystals. *Phys. Rev. B* **37,** 4458–4472 (1988).
6. Ishii, Y. Phason softening and structural transitions in icosahedral quasicrystals. *Phys. Rev. B* **45,** 5228–5239 (1992).
7. Henley, C. L. in *Quasicrystals: The State of the Art* (eds DiVincenzo, D. & Steinhardt, P. J.) 429–524 (World Scientific, Singapore, 1991).
8. Jeong, H. C. & Steinhardt, P. J. Finite-temperature elasticity phase transition in decagonal quasicrystals. *Phys. Rev. B* **48,** 9394–9403 (1993).
9. Bancel, P. A. in *Quasicrystals: The State of the Art* (eds DiVincenzo, D. & Steinhardt, P. J.) 17–55 (World Scientific, Singapore, 1991).
10. Colella, R., Zhang, Y., Sutter, J. P., Ehrlich, S. N. & Kycia, S. W. Debye-Waller factors in a quasicrystal. *Phys. Rev. B* **63,** 014202 (2000).
11. Dolinsek, J., Apih, T., Simsic, M. & Dubois, J. M. Self-diffusion in icosahedral $Al_{72.4}Pd_{20.5}Mn_{7.1}$ and phason percolation at low temperatures studied by ^{27}Al NMR. *Phys. Rev. Lett.* **82,** 572–575 (1999).
12. Coddens, G. & Steurer, W. Time-of–flight neutron-scattering study of phason hopping in decagonal Al-Co-Ni quasicrystals. *Phys. Rev. B* **60,** 270–276 (1999).
13. Edagawa, K., Suzuki, K. & Takeuchi, S. High resolution transmission electron microscopy observation of thermally fluctuating phasons in decagonal Al-Cu-Co. *Phys. Rev. Lett.* **85,** 1674–1677 (2000).
14. de Boissieu, M. *et al.* Diffuse scattering and phason elasticity in the AlPdMn icosahedral phase. *Phys. Rev. Lett.* **75,** 89–92 (1995).
15. Zeger, G., Plachke, D., Carstanjen, H. D. & Trebin, H.-R. Quasicrystalline d-AlCuCo identified as random tiling by ion channeling combined with particle-induced X-ray emission. *Phys. Rev. Lett.* **82,** 5273–5276 (1999).
16. Pennycook, S. J. & Jesson, D. E. High-resolution Z-contrast imaging of crystals. *Ultramicroscopy* **37,** 14–38 (1991); Atomic-resolution Z-contrast imaging of interfaces. *Acta Metall. Mater.* **40,** S149–S159 (1992).
17. Muller, D. A., Edward, B., Kirkland, E. J. & Silcox, J. Simulation of thermal diffuse scattering including a detailed phonon dispersion curve. *Ultramicroscopy* **86,** 371–380 (2001).
18. Ritsch, S. *et al.* Highly perfect decagonal Al-Co-Ni quasicrystal. *Phil. Mag. Lett.* **74,** 99–106 (1996).
19. Saitoh, K. *et al.* Structural study of an $Al_{72}Ni_{20}Co_8$ decagonal quasicrystal using the high-angle annular dark-field method. *Jpn. J. Appl. Phys.* **36,** L1400–L1402 (1997).
20. Yan, Y., Pennycook, S. J. & Tsai, A. P. Direct imaging of local chemical disorder and columnar vacancies in ideal decagonal Al-Ni-Co quasicrystals. *Phys. Rev. Lett.* **81,** 5145–5148 (1998).
21. Steinhardt, P. J. *et al.* Experimental verification of the quasi-unit-cell model of quasicrystal structure. *Nature* **396,** 55–57 (1998); correction *Nature* (**399**), 84 (1999).
22. Gummelt, P. Construction of Penrose tilings by a single aperiodic protoset. *Geom. Dedicata* **62,** 1–17 (1996).
23. Abe, E. *et al.* Quasi-unit cell model for an Al-Ni-Co ideal quasicrystal based on clusters with broken tenfold symmetry. *Phys. Rev. Lett.* **84,** 4609–4612 (2000).
24. Yan, Y. & Pennycook, S. J. Chemical ordering in $Al_{72}Ni_{20}Co_8$ decagonal quasicrystals. *Phys. Rev. Lett.* **86,** 1542–1545 (2001).
25. Abe, H. *et al.* Anomalous Debye-Waller factor associated with an order-disorder transformation in an $Al_{72}Ni_{20}Co_8$ decagonal quasicrystal. *J. Phys.* (submitted).
26. Henley, C. L., Mihalkovic, M. & Widom, M. Total-energy-based prediction for d(AlNiCo). *J. Alloys Comp.* **342,** 221–227 (2002).
27. Takakura, H., Yamamoto, A. & Tsai, A. P. The structure of decagonal $Al_{72}Ni_{20}Co_8$ quasicrystal. *Acta Crystallogr. A* **57,** 576–585 (2001).
28. Cervellino, A., Haibach, T. & Steurer, W. Structure solution of the basic decagonal Al-Co-Ni phase by the atomic surfaces modeling method. *Acta Crystallogr. B* **58,** 8–33 (2002).
29. Hiraga, K., Ohsuna, T. & Nishimura, S. An ordered arrangement of atom columnar clusters in a pentagonal quasiperiodic lattice of an Al-Ni-Co decagonal quasicrystal. *Phil. Mag. Lett.* **80,** 653–659 (2000).
30. Weickenmeier, A. & Kohl, H. Computation of absorptive form factors for high-energy electron diffraction. *Acta Crystallogr. A* **47,** 590–597 (1991).

Acknowledgements We thank H. Takakura, T. J. Sato, N. Tanaka, K. Ishizuka, M. Widom and C. L. Henley for discussions.

Competing interests statement The authors declare that they have no competing financial interests.

Correspondence and requests for materials should be addressed to E.A. (e-mail: abe.eiji@nims.go.jp).

Photocontrolled reversible release of guest molecules from coumarin-modified mesoporous silica

Nawal Kishor Mal, Masahiro Fujiwara & Yuko Tanaka

Kansai Center, National Institute of Advanced Industrial Science and Technology (AIST-Kansai), Ikeda, Osaka 563-8577, Japan

Since the discovery[1] of MCM-41 more than ten years ago, many investigations have explored the suitability of hexagonal mesoporous silicas for potential practical applications[2–4]. These range from catalysis[5,6] and optically active materials[7,8] to polymerization science[9–12], separation technology[3,13,14] and drug delivery[15–18], with recent successes in the fabrication of hybrid mesoporous organosilicas[19–21] expected to open up further application possibilities. Because the pore voids of this class of materials exhibit relatively narrow pore size distributions in the range of 2–4 nm in diameter, mesoporous silicas can selectively include organic compounds and release them continuously at a later stage. The functionalization of MCM-41 pore voids with photoactive derivatives[22–25] provides influence over the material's absorption behaviour, but full control over the release process remains difficult. Here we show that the uptake, storage and release of organic molecules in MCM-41 can be regulated through the photocontrolled and reversible intermolecular dimerization[26,27] of coumarin derivatives attached to the pore outlets. Successful functionalization requires uncalcined MCM-41 still filled with the template molecules that directed the formation of its pores, to ensure that coumarin derivatives attach preferentially to the pore outlets, rather than their inside walls. We find that this feature and the one-dimensional, isolated nature of the individual pores allow for efficient and reversible photocontrol over guest access to the material's interior.

The preparation of MCM-41 modified with a substituent bearing a coumarin group used as-synthesized MCM-41 and 7-[(3-triethoxysilyl)propoxy]coumarin (for full details, see Methods). Sample **1A** consists of MCM-41 with 4.0 wt% coumarin substituent. The molecular length of 7-[(3-trihydroxysilyl)propoxy]coumarin, attached to silanol groups on MCM-41, is approximately 1.3 nm (see Supplementary Information); dimerization should yield cyclobutane coumarin dimers in anti head-to-head configuration and sufficiently long[27] to obstruct the entrances to the pore of MCM-41 (pore diameter ~3 nm).

The ultraviolet (UV) diffuse reflectance spectrum of coumarin-modified MCM-41 (sample **1A**) is shown as a bold line in Fig. 1a. The absorption of the coumarin part (wavelength of maximum absorption $\lambda_{max} = 324$ nm) is clearly visible, confirming the successful grafting of coumarin substituents. Solid-state ^{29}Si NMR spectra also confirm grafting of organic molecules to the silica (Supplementary Information).

Irradiation of sample **1A** with UV light with wavelengths longer than 310 nm induces photodimerization, and thus results in a gradual decrease in the absorption band centred at 324 nm; the adsorption has almost disappeared after 50 min (Fig. 1a). In contrast, irradiation with UV light with a wavelength around 250 nm regenerates the coumarin absorption band within 2–3 min, owing to photocleavage of the coumarin dimers; however, the absorption feature decreases again under prolonged irradiation (Fig. 1b).

We regard the coumarin substituents as 'hinged double doors' controlling access to the pores of MCM-41. In the absence of any photo-irradiation and after photocleavage of the dimers (when the coumarin substituents are present as monomers), the 'double doors' are open and allow access to the interior of MCM-41. After photodimerization, the double doors are closed, with cyclobutane dimers spanning the pore entrances and obstructing access—the pore void is isolated. In contrast, the reversible photochromism effects reported for diazo[8,23] and spiropyran derivatives[24,25] attached to mesoporous materials are not expected to regulate pore access: in many cases, the optically active molecules are incorporated inside the pores, and the reactions are intramolecular and thus give rise to significantly smaller changes in the extent of pore obstruction.

Controlled-release experiments are conducted with the steroid cholestane, because its molecular size (~1.9 nm length and ~0.6 nm diameter)[28] allows it to be stored in the pores of MCM-41. In addition, cholestane has no UV absorption band around 324 nm that would interfere with monitoring of coumarin spectra. The amount of cholestane absorbed in the pores of sample **2A** (MCM-41 modified with coumarin derivatives and exposed to light after guest entrance, to induce dimerization) was 28 wt% (see Methods and Table 1). Washing in the absence of irradiation resulted in no cholestane remaining in the modified MCM-41. Unmodified MCM-41 also failed to retain cholestane after washing. Similarly, photo-induced dimerization of the coumarin-modified MCM-41 (sample **1A**) before exposure to guest solution resulted in no cholestane being absorbed in the material. These observations suggest that cholestane is retained in modified MCM-41 owing to cyclobutane coumarin dimers preventing passage through the pore outlets.

Sample **2A** was then irradiated with UV light with a wavelength of around 250 nm to cleave the cyclobutane rings, yielding sample **3A**. Washing with *n*-hexane released 77% of the stored cholestane to the solution. To our knowledge, this is the first demonstration of active control over the accessibility of the pores in mesoporous silica.

Table 1 summarizes essential features of the different MCM-41 samples. As indicated, X-ray diffraction measurements (see also Supplementary Information) showed no difference between the MCM-41 samples (samples **1A–3A** and without modification), indicating that the hexagonal silica structure and pore features are not influenced by the coumarin-modification, photo-irradiation, and the cholestane storage/release process. The nitrogen adsorption–desorption isotherms (Fig. 2), however, exhibit distinct differences: whereas coumarin-modification has no influence on nitrogen uptake and release by sample **1A**, coumarin photodimerization (yielding sample **2A**) and subsequent photocleavage (yielding sample **3A**) influence these properties (Fig. 2; for pore size distribution data, see Supplementary Information). As illustrated in the figure, cholestane storage in the pores of the photodimerized sample leads to a very marked decrease in the amount of adsorbed nitrogen (sample **2A**), with the specific surface area and pore volume reduced to a quarter of the values seen for sample **1A**. UV-induced ring cleavage and washing with *n*-hexane, to give sample **3A,** increases the specific surface area as well as the pore volume, as expected if the washing treatment releases most of the cholestane from the MCM-41 pores to the *n*-hexane solution. This process is complete after 48 h (releasing rate; see Supplementary Information). Because the photocleavage of the coumarin dimers proceeds imperfectly[26,27], some cholestane is expected (and is

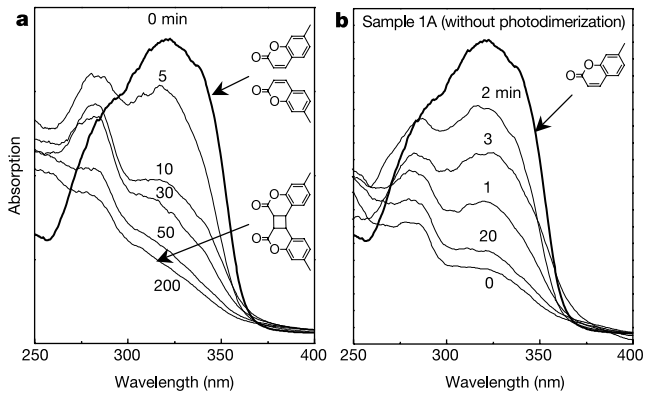

Figure 1 Changes in UV–visible spectra of modified MCM-41 samples during UV irradiation. **a**, Sample **1A** (MCM-41 with 4 wt% coumarin substituent, prepared with a grafting time of 15 min; see Methods) during photo-irradiation with UV light of wavelength >310 nm. **b**, Sample **2A** (cholestane absorbed to sample **1A**, followed by photodimerization and washing) during photo-irradiation with UV light of wavelength around 250 nm. The structures of coumarin monomer and dimer are also shown, and the spectra corresponding to the presence of only monomers or dimers are identified.

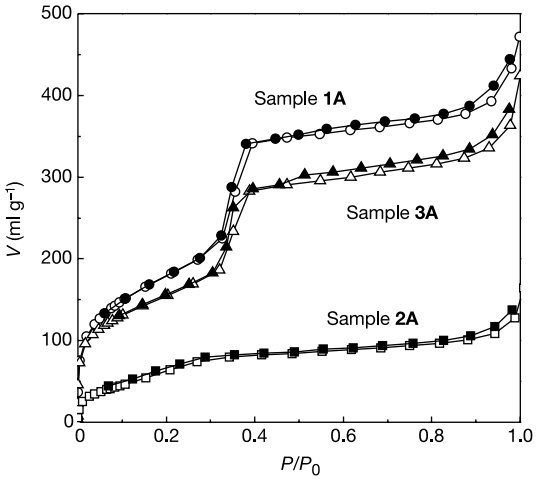

Figure 2 Nitrogen adsorption–desorption isotherms of MCM-41 samples. Shown are data for sample **1A** (see Fig. 1 legend), sample **2A** (see Fig. 1 legend) and sample **3A** (photocleaved and washed sample **2A**). *V*, volume of N_2 adsorbed; *P*, pressure of adsorbent; P_0, saturation pressure (1 atm). Open symbols, adsorption branch of isotherm; closed symbols, desorption branch of isotherm.

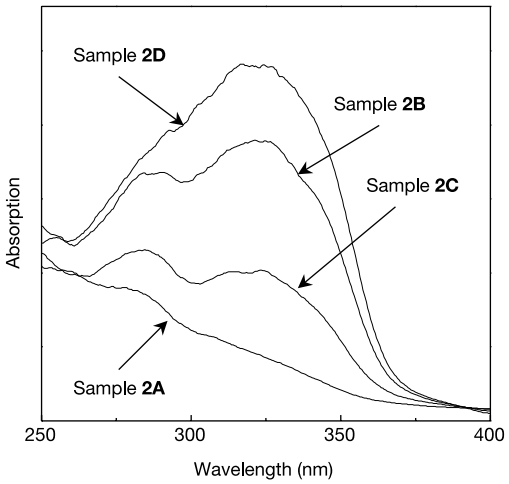

Figure 3 UV–visible spectra of coumarin-modified MCM-41 after complete photo-irradiation by UV light of wavelength >310 nm. Data are shown for sample **2A** (see Fig. 1 legend), sample **2B** (cholestane absorbed, photodimerized and washed 5.6 wt% coumarin grafted MCM-41; grafting time, 22 h), sample **2C** (cholestane absorbed, photodimerized and washed 4 wt% coumarin grafted on calcined MCM-41 for 15 min) and sample **2D** (cholestane absorbed, photodimerized and washed 5.6 wt% coumarin grafted MCM-41 produced by one-pot synthesis).

observed) to remain in the pores (Table 1). Comparable uptake and release behaviour was observed with pyrene and phenanthrene, molecules that are smaller than cholestane. Similarly, the uptake and release of progesterone, a corpus luteum hormone, could also be controlled (after photodimerization: 28.2 wt% storage, and after photocleavage: 6.0 wt% storage).

To achieve effective release control, the coumarin substituents need to be attached to the pore outlets of the modified MCM-41. This was achieved by modifying as-synthesized MCM-41 at ambient temperature (~295 K) over a short grafting time (15 min). When using identical conditions except for a grafting time of 22 h (sample **1B**; 5.6 wt% grafted), the material exhibited significantly worse performance in controlled uptake and release experiments (Table 1, samples **2B** and **3B**). Similarly, when an equal amount of coumarin substituent was grafted in a short period (15 min) to calcined MCM-41 (sample **1C**; 4.0 wt% grafted), cholestane uptake was significantly diminished (Table 1, samples **2C** and **3C**). Finally, coumarin-modified MCM-41 was also prepared by one-pot hydrothermal synthesis (sample **1D**; 5.6 wt% grafted), but showed no evidence for controlled release after extraction of the surfactant, or of cholestane storage after photo-irradiation (Table 1, sample **2D**).

Figure 3 gives the UV spectra of samples **2A**, **2B**, **2C** and **2D** after photo-irradiation (at wavelengths >310 nm) over 200 min. In the case of sample **2A**, the coumarin absorption at 324 nm has almost disappeared, indicating complete dimerization of coumarin (>98%). In the case of sample **2B** and **2C**, the less-pronounced decrease in the absorption at 324 nm indicates poor (25%) and incomplete (63%) dimerization, respectively, while sample **2D** shows essentially no evidence for photodimerization (<1%). These results indicate that, as expected, the position of the coumarin substituents in the pore of MCM-41 determines their reactivity to photodimerization. That is, the crowding of coumarin substituents at the pore outlets in sample **1A** enables almost complete photo-dimerization, whereas the more dispersed attachment in samples **2B** and **2C** allows for only limited coumarin photodimerization. In the case of sample **2B**, which used as-synthesized MCM-41, the long grafting time permits gradual displacement of surfactants and diffusion of coumarin reagents into the inner pore space. (More than 90% of the template was removed after this procedure). In the case of sample **2C**, grafting[29] on calcined MCM-41 but only over a short period resulted in preferential attachment near the outlet of the pores[30,31]. We expect that the large size of the coumarin substituents that we used, and their associated slow diffusion, will have enhanced this tendency, thus explaining the overall better

Table 1 **Properties of various modified MCM-41 samples**

Sample	Status	d_{100}* (nm)	S_{BET}† ($m^2 g^{-1}$)	V_p‡ ($cm^3 g^{-1}$)	APD§ (nm)	Peak pore diameter¶ (nm)	Cholestane storage (wt%)
MCM-41	Unmodified	4.06	982	0.84	2.80	3.0	0.0
Sample **1A**#	Modified	4.06	970	0.82	2.79	3.0	0.0
Sample **2A**	Dimerized	4.06	275	0.21	1.99	1.9	28.0
Sample **3A**	Cleaved	4.06	747	0.61	2.60	2.8	6.4
Sample **1B**☆	Modified	4.06	907	0.74	2.71	2.7	0.0
Sample **2B**	Dimerized	4.06	790	0.58	2.43	2.6	4.8
Sample **3B**	Cleaved	4.06	842	0.70	2.69	2.8	1.4
Sample **1C****	Modified	4.04	916	0.77	2.74	2.8	0.0
Sample **2C**	Dimerized	4.04	615	0.49	2.42	2.3	12.8
Sample **3C**	Cleaved	4.04	798	0.70	2.72	2.8	2.1
Sample **1D**‡‡	Modified	3.95	853	0.62	2.38	2.2	0.0
Sample **2D**	Dimerized	3.95	856	0.62	2.38	2.2	< 0.1

*d_{100}: X-ray diffraction (100) interplanar spacing.
†S_{BET}: BET specific surface area.
‡V_p: Primary mesopore volume.
§APD: average pore diameter = $4V_p/S_{BJH}$, where S_{BJH} is the BJH specific surface area.
‖Peak pore diameter calculated from BJH pore size distribution curve using adsorption branches.
¶Weight per cent of cholestane stored in the modified MCM-41 materials after thorough washing with *n*-hexane.
#Sample **A**: 4 wt% coumarin grafted MCM-41; grafting time, 15 min.
☆Sample **B**: 5.6 wt% coumarin grafted MCM-41; grafting time, 22 h.
Sample **C: 4 wt% coumarin grafted on calcined MCM-41 for 15 min.
‡‡Sample **D**: 5.6 wt% coumarin grafted in one-pot synthesis.

controlled-release performance of sample **2C**, relative to that of sample **2B** (Table 1). Of course, we expect that the entire external surface of all these modified MCM-41 samples has been functionalized during treatment with the coumarin derivatives, but this should not affect the performance of the materials in our controlled-release experiments. Finally, in the modified MCM-41 sample produced by one-pot synthesis (sample **2D**), the coumarin substituents are expected to exist randomly in the pore space, with this highly dispersed placement of the substituents preventing photodimerization of coumarin groups and the storage of chemicals in the pore.

The use of as-synthesized MCM-41 and a short time of grafting are essential for preparing materials that allow effective and direct control over guest uptake and release. Porous materials with interconnected pore architectures, such as silica gels, are expected to be less effective, because guest molecules could diffuse to the outside through remaining unmodified (not closed) pore outlets. Indeed, controlled release using coumarin-modified silica gel was not successful: although the photodimerization took place, no cholestane was stored in the gel. The present work shows that the isolated, one-dimensional cylindrical pores of MCM-41 render this material particularly suitable for controlled-release applications. □

Methods

Preparation of the coumarin-modified MCM-41

MCM-41 was prepared using gel of the following molar composition; 1 SiO_2: 0.51 CTMABr: 0.67 TMAOH: 0.46 Na_2O: 0.65 H_2SO_4: 80 H_2O (pH 9.75). The gel was heated at 373 K for 3 d. The obtained material was filtered off, washed and dried at 373 K for 24 h. 2 g of as-synthesized MCM-41 was suspended in a solution containing 20 ml of *n*-hexane and 0.20 g of 7-[(3-triethoxysilyl)propoxy]coumarin under stirring at ambient temperature for 15 min. *n*-Hexane was evaporated by a rotary evaporator at 353 K for 2 h, and the resulting material was dried under vacuum at 423 K for 12 h. 2 g of this coumarin-modified as-synthesized MCM-41 with surfactant was refluxed in 100 ml of ethanol containing 4 ml of HCl (1 M) at 353 K for 4 h. The solid was descended and washed with ethanol. This process was carried out twice to ensure the complete removal of surfactant from the pores of MCM-41. The obtained solid was filtered off, washed with ethanol and water, and finally dried at 353 K for 12 h. This material was referred as sample **1A**. Sample **1B** was prepared by the same grafting procedure as sample **1A** for 22 h duration. Sample **1C** was obtained by grafting 4.0 wt% of coumarin substituent on calcined MCM-41 at ambient temperature in hexane solution under stirring for 15 min. Sample **1D** was synthesized from the mixed solution of tetraethoxysilane and 7-[(3-triethoxysilyl)propoxy]coumarin (5 mol% to tetraethoxysilane) by the same procedure as mentioned above. The removal of surfactant and the amount of substituents in MCM-41 were assessed by gas chromatography, thermogravimetric analysis, and chemical analysis.

Preparation of 7-[(3-triethoxysilyl)propoxy]coumarin

7-Allyloxycoumarin was obtained from umberiferon and allyl bromide in the presence of potassium carbonate, and purified by recrystallization from ethanol. The yield was over 90%. 7-[(3-triethoxysilyl)propoxy]coumarin was prepared as follows; after bubbling dry nitrogen into a toluene solution (100 ml) of 7-allyloxycoumarin 3.24 g (16 mmol) and triethoxysilane 2.94 g (17.6 mmol) for 10 min, 0.8 ml of a toluene solution (2 mM) of Pt (dvs) [platinum(0)-1,3-divinyl-1,1,3,3-tetramethyldisiloxane complex] (Aldrich) was added, and the resulting solution was stirred for 12 h at room temperature. After removing solvent under reduced pressure, the oil obtained (successfully identified as 7-[(3-triethoxysilyl)propoxy]coumarin) was used directly to modify MCM-41.

Photoresponsive on-off controlled-release experiment

1 g of coumarin-modified MCM-41 (samples **1A, 1B, 1C** and **1D**) was suspended in an *n*-hexane solution (20 ml) containing 1 g of cholestane at ambient temperature for 24 h. The resulting solid was filtered off, washed with *n*-hexane many times on a filter, and dried at 333 K for 12 h. The content of cholestane in the filtrate was analysed using gas chromatography. The obtained solid was photodimerized by irradiation with UV light of wavelength >310 nm for 30 min using a 450-W high-pressure mercury lamp through a Pyrex glass cooler. After the dimerization, the solid was suspended in *n*-hexane (100 ml) and stirred at room temperature for 48 h. Finally, the solid was filtered off, washed with *n*-hexane and dried at room temperature (samples **2A, 2B, 2C** and **2D**). The amounts of cholestane in samples **2A, 2B, 2C** and **2D** were estimated from the difference between the initial and the recovered amounts. This dimerized material was subjected to photocleavage by irradiation at around 250 nm wavelength for 2.5 min with a low-pressure mercury lamp through a quartz glass cooler, and treated with *n*-hexane (100 ml) at room temperature under stirring for 48 h. Finally, the solid was descended, washed and dried at room temperature (samples **3A, 3B** and **3C**). The amounts of cholestane released (dissolved in *n*-hexane) were analysed using gas chromatography and thermogravimetric analysis.

Received 7 June; accepted 10 December 2002; doi:10.1038/nature01362.

1. Kresge, C. T., Leonowicz, M. E., Roth, W. J., Vartuli, J. C. & Beck, J. S. Ordered mesoporous molecular sieves synthesized by a liquid-crystal template mechanism. *Nature* **359,** 710–712 (1992).
2. Ying, J. Y., Mehnert, C. P. & Wong, M. S. Synthesis and applications of supramolecular-templated mesoporous materials. *Angew. Chem. Int. Edn Engl.* **38,** 56–77 (1999).
3. Stein, A., Melde, B. J. & Schroden, R. C. Hybrid inorganic-organic mesoporous silicates—Nanoscopic reactors coming of age. *Adv. Mater.* **12,** 1403–1419 (2000).
4. Davis, M. E. Ordered porous materials for emerging applications. *Nature* **417,** 813–821 (2002).
5. Maschmeyer, T., Rey, F., Sanker, G. & Thomas, J. M. Heterogeneous catalysts obtained by grafting metallocene complexes onto mesoporous silica. *Nature* **378,** 159–162 (1995).
6. Corma, A. From microporous to mesoporous molecular sieve materials and their use in catalysis. *Chem. Rev.* **97,** 2373–2419 (1997).
7. Nguyen, T. Q., Wu, J. J., Doan, V., Schwartz, B. J. & Tolbert, S. H. Control of energy transfer in oriented conjugated polymer-mesoporous silica composites. *Science* **288,** 652–656 (2000).
8. Ganschow, M., Wark, M., Wohrle, D. & Schulz-Ekloff, G. Anchoring of functional dye molecules in MCM-41 by microwave-assisted hydrothermal co-condensation. *Angew. Chem. Int. Edn Engl.* **39,** 161–163 (2000).
9. Wu, C. G. & Bein, T. Conducting polyaniline filaments in a mesoporous channel host. *Science* **264,** 1757–1759 (1994).
10. Zhou, W. Z. *et al.* Ordering of ruthenium cluster carbonyls in mesoporous silica. *Science* **280,** 705–708 (1998).
11. Kageyama, K., Tamazawa, J. & Aida, T. Extrusion polymerization: Catalyzed synthesis of crystalline linear polyethylene nanofibers within a mesoporous silica. *Science* **285,** 2113–2115 (1999).
12. Spange, S. *et al.* Cationic host-guest polymerization of N-vinylcarbazole and vinyl ethers in MCM-41, MCM-48, and nanoporous glasses. *Chem. Eur. J. A* **7,** 3722–3728 (2001).
13. Feng, X. *et al.* Functionalized monolayers on ordered mesoporous supports. *Science* **276,** 923–926 (1997).
14. Mercier, L. & Pinnavaia, T. J. Access in mesoporous materials: Advantages of a uniform pore structure in the design of a heavy metal ion adsorbent for environmental remediation. *Adv. Mater.* **9,** 500–503 (1997).
15. Ahola, M., Kortesuo, P., Kangasniemi, I., Kiesvaara, J. & Antti Yli-Urpo, A. Silica xerogel carrier material for controlled release of toremifene citrate. *Int. J. Pharm.* **195,** 219–227 (2000).
16. Arcos, D., Ragel, C. V. & Vallet-Regí, M. Bioactivity in glass/PMMA composites used as drug delivery system. *Biomaterials* **22,** 701–708 (2001).
17. Czuryszkiewicz, T. *et al.* Drug release from biodegradable silica fibers. *J. Non-Cryst. Solids* **306,** 1–10 (2002).
18. Vallet-Regi, M., Rámila, A., del Real, R. P. & Pérez-Pariente, J. A new property of MCM-41: Drug delivery system. *Chem. Mater.* **13,** 308–311 (2001).
19. Asefa, T., MacLachan, M. J., Coombs, N. & Ozin, G. A. Periodic mesoporous organosilicas with organic groups inside the channel walls. *Nature* **402,** 867–871 (1999).
20. Fujiwara, M. *et al.* Preparation of MCM-41/nafion composite material; a selective catalyst of α-methylstyrene dimerization. *J. Chem. Soc. Chem. Commun.* 1523–1524 (2000).
21. Inagaki, S., Guan, S., Ohsuna, T. & Terasaki, O. An ordered mesoporous organosilica hybrid material with a crystal-like wall structure. *Nature* **416,** 304–307 (2002).
22. Alvaro, M., Ferrer, B., García, H. & Rey, F. Photochemical modification of the surface area and tortuosity of a *trans*-1,2-bis(4-pyridyl)ethylene periodic mesoporous MCM organosilica. *J. Chem. Soc. Chem. Commun.* 2012–2013 (2002).
23. Hoffmann, K., Resch-Genger, U. & Marlow, F. Photoinduced switching of nanocomposites consisting of azobenzene and molecular sieves: Investigation of the switching states. *Micropor. Mesopor. Mater.* **41,** 99–106 (2000).
24. Wirnsberger, G., Scott, B. J., Chmelka, B. F. & Stucky, G. D. Fast response photochromic mesostructures. *Adv. Mater.* **12,** 1450–1454 (2000).
25. Schomburg, C., Wark, M., Rohlfing, Y., Schulz-Ekloff, G. & Wöhrle, D. Photochromism of spiropyran in molecular sieve voids: Effects of host-guest interaction on isomer status, switching stability and reversibility. *J. Mater. Chem.* **11,** 2014–2021 (2001).
26. Chujo, Y., Sada, K. & Saegusa, T. Polyoxazoline having a coumarin moiety as a pendant group. Synthesis and photogelation. *Macromolecules* **23,** 2693–2697 (1990).
27. Li, W. J., Lynch, V., Thompson, H. & Fox, M. A. Self-assembled monolayers of 7-(10-thiodecoxy)coumarin on gold: Synthesis, characterization, and photodimerization. *J. Am. Chem. Soc.* **119,** 7211–7217 (1997).
28. Berezin, M. Y., Dzenitis, J. M., Hughes, B. M. & Ho, S. V. Separation of sterols using zeolites. *Phys. Chem. Chem. Phys.* **3,** 2184–2189 (2001).
29. Kruk, M., Antochshuk, V., Matos, J. R., Mercuri, L. P. & Jaroniec, M. Determination and tailoring the pore entrance size in ordered silicas with cage-like mesoporous structures. *J. Am. Chem. Soc.* **124,** 768–769 (2002).
30. Zhao, X. S., Lu, G. Q. M. & Hu, X. A novel method for tailoring the pore-opening size of MCM-41 materials. *J. Chem. Soc. Chem. Commun.* 1391–1392 (1999).
31. Lim, M. H. & Stein, A. Comparative studies of grafting and direct syntheses of inorganic-organic hybrid mesoporous materials. *Chem. Mater.* **11,** 3285–3295 (1999).

Supplementary Information accompanies the paper on *Nature*'s website (**http://www.nature.com/nature**).

Acknowledgements N.K.M. was supported by an STA fellowship.

Competing interests statement The authors declare that they have no competing financial interests.

Correspondence and requests for materials should be addressed to M.F. (e-mail: m-fujiwara@aist.go.jp).